ORIGINAL RESEARCH

Composite Hydrogel Dressings with Enhanced Mechanical Properties and Anti-Inflammatory Ability for Effectively Promoting Wound Repair

Yuqin Feng[1,2], Si Qin[3], Huarun Li[3], Yemei Yang[1], Yushi Zheng[1], Hongsheng Liu[4], Wei Yin Yap[1,5], Xianyi Zhou [1], Ju Wen[2,3]

[1]Department of Dermatology, the Third Affiliated Hospital of Southern Medical University, Guangzhou, 510630, People's Republic of China; [2]The Second School of Clinical Medicine, Southern Medical University, Guangzhou, 510280, People's Republic of China; [3]Department of Dermatology, Guangdong Second Provincial General Hospital, Guangzhou, 510317, People's Republic of China; [4]Guangdong Huace Life Medicine Research Center, Guangzhou, 511450, People's Republic of China; [5]School of International Education of Southern Medical University, Guangzhou, 510515, People's Republic of China

Correspondence: Xianyi Zhou; Ju Wen, Email zxy1962@163.com; wenju3139@163.com

Background: Hydrogel dressings have been used as a crucial method to keep the wound wet and hasten the healing process. Due to safety concerns regarding the gel components, low mechanical adhesiveness, and unsatisfactory anti-inflammatory capacity qualities for practical uses in vivo, leading to the clinical translation of wound dressings is still difficult.
Methods: A type of composite hydrogel (acrylamide/polyethylene glycol diacrylate/tannic acid, ie, AM/PEGDA/TA) by double bond crosslinking, Schiff base, and hydrogen bond interaction is proposed. The mechanical characteristics, adhesiveness, and biocompatibility of the hydrogel system were all thoroughly examined. Additionally, a full-thickness cutaneous wound model was employed to assess the in vivo wound healing capacity of resulting hydrogel dressings.
Results: Benefiting the mechanism of multiple crosslinking, the designed composite hydrogels showed significant mechanical strength, outstanding adhesive capability, and good cytocompatibility. Moreover, the hydrogel system also had excellent shape adaptability, and they can be perfectly integrated into the irregularly shaped wounds through a fast in situ forming approach. Additional in vivo tests supported the findings that the full-thickness wound treated with the composite hydrogels showed quicker epithelial tissue regeneration, fewer inflammatory cells, more collagen deposition, and greater levels of platelet endothelial cell adhesion molecule (CD31) expression.
Conclusion: These above results might offer a practical and affordable product or method of skin wound therapy in a medical context.
Keywords: hydrogel dressing, tannins, multiple-crosslinking, anti-inflammatory, full-thickness wound healing

Introduction

Trauma is a very prevalent clinical disease that is brought on by cuts, burns, scalds, and diabetes and has a significant negative impact on people's health and quality of life.[1–5] Extreme trauma can lead to significant issues in clinical practice. Infection and bleeding are constant problems in wound care, and they can result in shock, incapacity, or even death.[6] When bacteria colonize the damaged skin of a wound, a wound infection results, which can cause pain, swelling, and redness around the site.[7,8] Wound hemostasis and the use of biomaterials for post-injury dressings are particularly crucial for ensuring quick and healthy wound healing. The creation of multifunctional, high-performance hemostatic polymers to control wound infection and bleeding has long been on the horizon.[9–11]

Due to their analogous properties similar to those of the natural extracellular matrix (ECM), which maintains a moist environment, hampers the loss of body fluids, protects the wound from microbial contamination, and generally expedites the healing process, various hydrogel wound dressings were particularly regarded as a promising and competitive

substitute for skin defect repair.[12–17] To date, various polymer hydrogel-based dressings, such as hyaluronic acid,[18] starch,[19] and sodium alginate,[20] have been widely reported to promote wound healing. However, natural polymeric hydrogels are mechanically weak and brittle, which severely restricts their use, while single-synthesized polymeric hydrogels often have considerable resistance to cell attachment. Consequently, it is important but difficult to create a composite hydrogel system with superior mechanical characteristics and biocompatibility.

It is well known that another crucial aspect of hydrogel as an appropriate wound dressing is its adhesive property. Catechol-based adhesions, which are motivated by mussel attachment on reefs, offer an intriguing candidate for strong adhesive design.[18,21–24] These adhesions are mediated by dynamic noncovalent interactions (such as hydrogen bonds, hydrophobic interactions, and cation interactions) as well as covalent bonds (such as coordination bonds, borate ester bonds, Michal additions, and Schiff base reactions).[25–27] Natural polyphenol tannic acid (TA) has pyrogallol groups, which are comparable to the catechol groups in dopamine.[28–30] Although there are more phenolic OH units in TA (25 per TA molecule) than there are in dopamine, this results in a quicker and more durable coating of TA on practically both inorganic and organic surfaces.[31–33] Thus, TA is acknowledged as a flexible and powerful molecular adhesive capable of forming multidentate contacts with polymer chains, resulting in a stable boundary barrier between the adhesive and a variety of substrates. On the other hand, PEG-based adhesives exhibited better mechanical characteristics as a result of covalent connections between TA and the amino groups of the protein. It is reasonable to assume that by reprogramming a cross-linked network, polymer network integration will further strengthen the adhesive strength of TA-polymer-based glue.

Herein, a kind of physicochemical multiple cross-linked multifunctional hydrogels (AM/PEGDA/TA) for full-thickness skin defect model wound healing was designed (Scheme 1). Specially, the AM/PEGDA/TA system was achieved by integrating interpenetrating network hydrogel with polyacrylamide (PAM), poly (ethylene glycol) diacrylate (PEGDA) and tannins (TA). The hydrogel network was composed of covalently cross-linked AM or PEGDA and reversible hydrogen bonds. Then, the rheology properties, mechanical performance, morphology, and adhesive characteristics were assessed. As a result, compared to single cross-linking, multiple cross-linking of the AM/PEGDA/TA hydrogels resulted in rapid gelling ability, interpenetrating network structure, reinforced mechanical property, and adhesive strength. The hydrogels also had excellent shape adaptability, and they can be perfectly integrated into the irregularly shaped wounds through an in situ forming approach because of their unique gelling behavior. Furthermore, the hydrogel system had adequate biocompatibility, as demonstrated by the cytotoxicity tests. The hydrogel was now suitable for the treatment of dynamic irregular wounds thanks to these improved characteristics. The in vivo results showed that the resultant hydrogel scaffolds had a synergistic effect of anti-inflammatory and vascularization on the healing of full-thickness cutaneous defects following animal tests on wound models. The AM/PEGDA/TA composite hydrogel systems may therefore have a bright future in the field of clinical wound care.
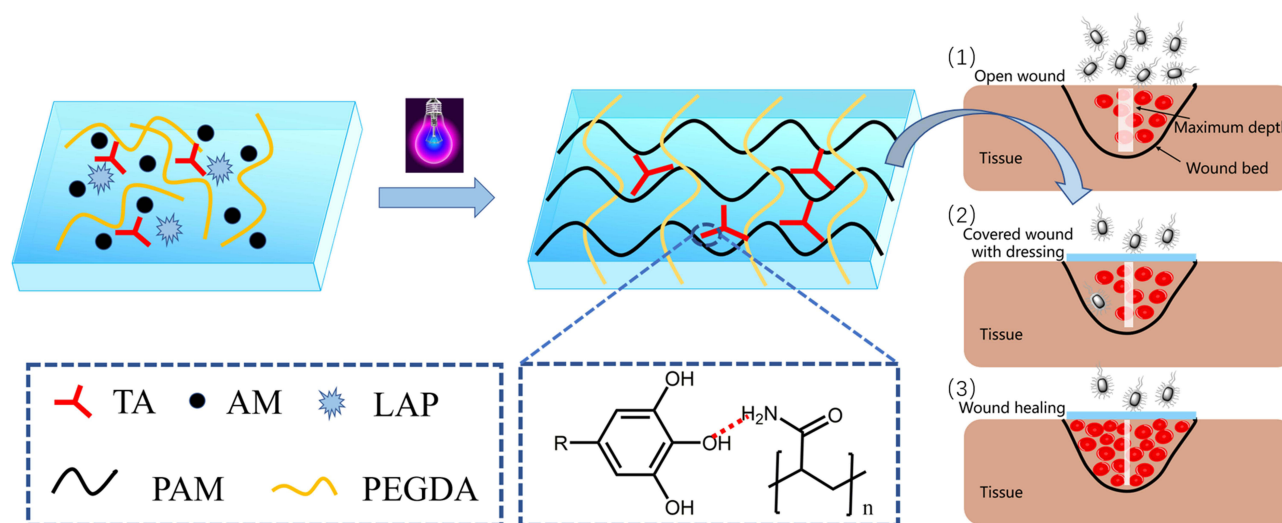
Scheme 1 Schematic illustration of the preparation of AM/PEGDA/TA composite hydrogel for promoting regeneration of full-thickness wound defects.

Experimental Section

Materials

PEG (M_n= 6000) was supplied by J&K Scientific Ltd., China. Lithium phenyl-2,4,6-trimethylbenzoylphosphinate (LAP a light initiator), potassium carbonate, tannin (TA), and acrylamide (AM) were obtained from Aladdin Reagent (China). Ultrapure water is used in all experiments. Other analytical reagents used in the present study were obtained from the Tianjin Damao Chemical Reagent Factory.

Synthesis of PEGDA

First, 24 g of PEG and 72 mL of anhydrous dichloromethane (which has been dehydrated with calcium hydride) were successively added into a 250 mL three-neck flask. After the PEG is completely dissolved, drop 0.5 mL of triethylamine (dried with sodium hydroxide) and 0.9 mL of acryloyl chloride successively under the conditions of 4°C and magnetic stirring, then poured N_2 into the reaction solution for protection, and continue to stir for 2 days; After the reaction is completed, add 20 mL (2 mol/L) of potassium carbonate solution to the reaction solution to remove hydrogen chloride generated in the container, and transfer it to the separating funnel. After the liquid is fully shaken, let it stand for 4 h to form a two-phase separating solution. Take the reaction solution at the bottom layer (dichloromethane phase) and add 0.5 g magnesium sulfate powder for drying. The supernatant was obtained by centrifugation and then concentrated into a light yellow viscous liquid. Then, ether was added until white powder samples were separated. The samples were filtered, collected, dried in a 25°C vacuum drying oven, and sealed and kept away from light. Finally, the chemical structure of products was analyzed by using attenuated total reflectance-Fourier transformation infrared (ATR-FTIR, Bruker Tensor 27, Germany) and Nuclear Magnetic Resonance (NMR) spectrometer (Bruker, AVANCEIII400MHz, Germany).

Preparation of AM/PEGDA/TA

AM (250 mg), PEGDA (100 mg) and TA (50 mg) were added into 10 mL of ultrapure water, followed by vigorous shaking using a vortex mixer at the maximum. Then, 0.1 mL of LAP solution (4%, w/v) was added to the mixture and continued to stir for 10 min at room temperature. After that, the above-resultant solution was transferred to the specific mold and exposed to Blu-ray irradiation (365 nm, 50 mW/cm^2) for 3 min to produce AM/PEGDA/TA composite hydrogel. For comparison, PEGDA and AM/PEGDA hydrogel were also prepared using the same method.

Rheological Test of Hydrogels

The rheological performance of hydrogels was measured on a rotational rheometer (DHR, TA Instruments, USA) at 37°C. The gelation time of the different hydrogel systems was studied via time sweeps (oscillatory strain of 1% and a frequency of 6.28 rad/s). Briefly, 1.0 mL hydrogel precursor has dropped from the testing platform and then was exposed to Blu-ray irradiation for detecting the change of storage modulus (G') and loss modulus (G") in the gelation process of the hydrogel.

Mechanical Evaluation of Hydrogels

An electronic universal testing machine (Shenzhen Suns Technology Stock Co, LTD.) was used to determine the tensile stress–strain curves of the hydrogels and the fabricated hydrogel scaffolds. To obtain the compressive or tensile stress–strain curve of the hydrogel specimens, the hydrogel was prepared as a cylinder (10 mm diameter and 8 mm height) or cut into dumbbell-shape (50 mm in length, 4 mm in width and 2 mm in thickness). Then, the crosshead on the top was moved upwards at a speed of 50 mm/min until the breaking of the hydrogel or reaching the operation limit of the machine. All tests are repeated three times.

Scanning Electron Microscope (SEM) Morphology Observation

After being lyophilized, the cross-sections of the scaffold specimens were coated with a gold layer and monitored by a SEM to study the morphologies and the pore sizes.

Adhesion Property Test

The adhesive forces of hydrogel to various substrates, including silicone rubber, plastic, stainless steel, porcine skin, and glass were evaluated using an electronic universal testing machine (Shenzhen Suns Technology Stock Co, LTD.). For testing the adhesion force of hydrogel to porcine skin, the two cover porcine skin slides (44 mm × 22 mm × 1mm, length × width × thickness) were used for the measurement. The hydrogel (~20 mg) was adhered to one substrate with a bond area of 15 mm × 15 mm, another substrate was then immediately placed over the hydrogel. Before the measurement, such attached substrates were left in the ambient environment for 5 min, and then the two substrates were pulled apart at a speed of 10 mm/min and the adhesion strengths were calculated as the measured maximum force divided by the applied bond area. All tests are repeated three times.

In vitro Cell Culture

The cell experiments were carried out using human umbilical vein endothelial cells (HUVECs, bought BeNa Culture Collection) owing to taking into account the influence of HUVECs on tissue revascularization. The HUVECs were cultured in Dulbecco's modified eagle medium supplemented with 10% FBS at 37°C in a humified atmosphere containing 5% CO_2. HUVECs were seeded in 96-well plates at a density of 8×10^3 cells/well until adherent and then were incubated with the different hydrogel materials at 37°C for 1, 3, and 5 days. Subsequently, MTT (1 mg/mL in medium, 100 μL/well) was added to the wells after the supernatant was removed followed by incubation at 37°C for 4 h. The supernatant was removed, and 100 μL DMSO per well was added to dissolve the produced formazan. After shaking the plates for 10 min, absorbance values of the wells were read with a microplate reader at 520 nm. The cell viability was calculated by the percentage of the absorbance of the experimental groups to the absorbance of the control group.

Then, live/dead staining was conducted with HUVECs which were planted into a 24-well plate with a density of 2×10^4 per well and cultured in DMEM medium containing 10% FBS under standard cell culture conditions for 12 hours. Then, the medium was replaced with fresh hydrogel, 100 μL PBS, or 1% Triton X-100 solution. The samples were further cultured at 37°C in a humidified atmosphere of 5% CO_2 for 3 days, respectively. After staining with 500 μL of calcein-AM/propidium iodide dye for 30 min, cells were observed under a fluorescent microscope for the green (492 nm) and red (545 nm) fluorescence. Besides, the morphology and cytoskeleton structure of HUVECs after incubation with different hydrogel samples were monitored by a CLSM. Specially, after culturing for 3 days, those treated cells were fixed in 4% paraformaldehyde, permeabilized by 0.1% Triton X-100, blocked with bovine serum albumin, and then immune stained with rhodamine-conjugated phalloidin (Life Technologies) for F-actin filament and 4',6-diamidino-2-phenylindole (DAPI, Life) for nucleus under dark condition.

In vivo Animal Experiments

All animal procedures were performed in accordance with the Guidelines for Care and Use of Laboratory Animals of Southern Medical University and approved by the Animal Ethics Committee of Southern Medical University. The assigned approval/accreditation number is SCXK(YUE)2020–0041. Male Kunming mice (5–6 weeks old) were purchased from the Guangdong Laboratory Animal Center. Each mouse was anesthetized intraperitoneally with 1% sodium pentobarbital. Then, the full-thickness wound including the panniculus carnosus muscle was made on the mid-back. After that, an 8 mm diameter punch biopsy instrument was placed with moderate force onto the dorsum of the mouse to create an impression of the circumference. Next, the middle of the outline region of skin was sharply excised along the outline with a pair of scissors. The excised tissue was full-thickness skin in depth, leaving the subcutaneous dorsal muscle exposed after excision. All the rats were divided into three groups (n = 5): PEGDA, AM/PEGDA and AM/PEGDA/TA hydrogel. After that, the wounds were treated, respectively, with 200 μL of the sterilized hydrogels pre-polymer solution, and then irradiated with Blu-ray light for 5 min, then the wounds in all groups were tightly wrapped with medical tape, and the rats were raised in cages individually at a standard temperature. Wound healing was observed and photographed at 0, 3, 7 and 14 days, and the wound area was determined by Image J software.

Histological Analysis

Wound tissue was gathered and fixed with 4% paraformaldehyde solution on days 3, 7 and 14. The obtained specimens were, respectively, stained with hematoxylin and eosin (H&E), immunohistochemical staining of IL-1β and IL-6, and double immunofluorescence staining of α-SMA (green) and CD31 (red) based on the standard protocol All the slices were analyzed and photographed using a microscope (IX53, Olympus, Japan).

Statistical Analysis

All data were obtained from at least triplicate tests and are showed as the mean ± SD. One-way ANOVA following Tukey's test was carried out for statistical analysis with GraphPad Prism software. The results were considered significant at $*p < 0.05$, $**p < 0.01$, and $***p < 0.001$, $n \geq 3$.

Results and Discussion

Synthesis and Characterization of AM/PEGDA/TA

First, the PEGDA polymer was synthesized by the previously reported method.[34,35] The successful preparation of PEGDA was proved by the analysis of ^{1}H MNR spectrum. As shown in Figure 1A, the PEGDA samples showed three different proton peaks in the range of chemical displacement 5.7–6.4 compared to the PEG, which belong to the three H proton peaks at both ends of the double bond of PEG after acrylation -CH = CH$_2$. Due to the appearance of these three peaks, it is confirmed that the terminal hydroxyl group of PEG is replaced by acrylate group, and another newly generated H proton peak appears near 4.3 ppm, which corresponds to the H proton peak of -CH$_2$O-CO- on the PEGDA
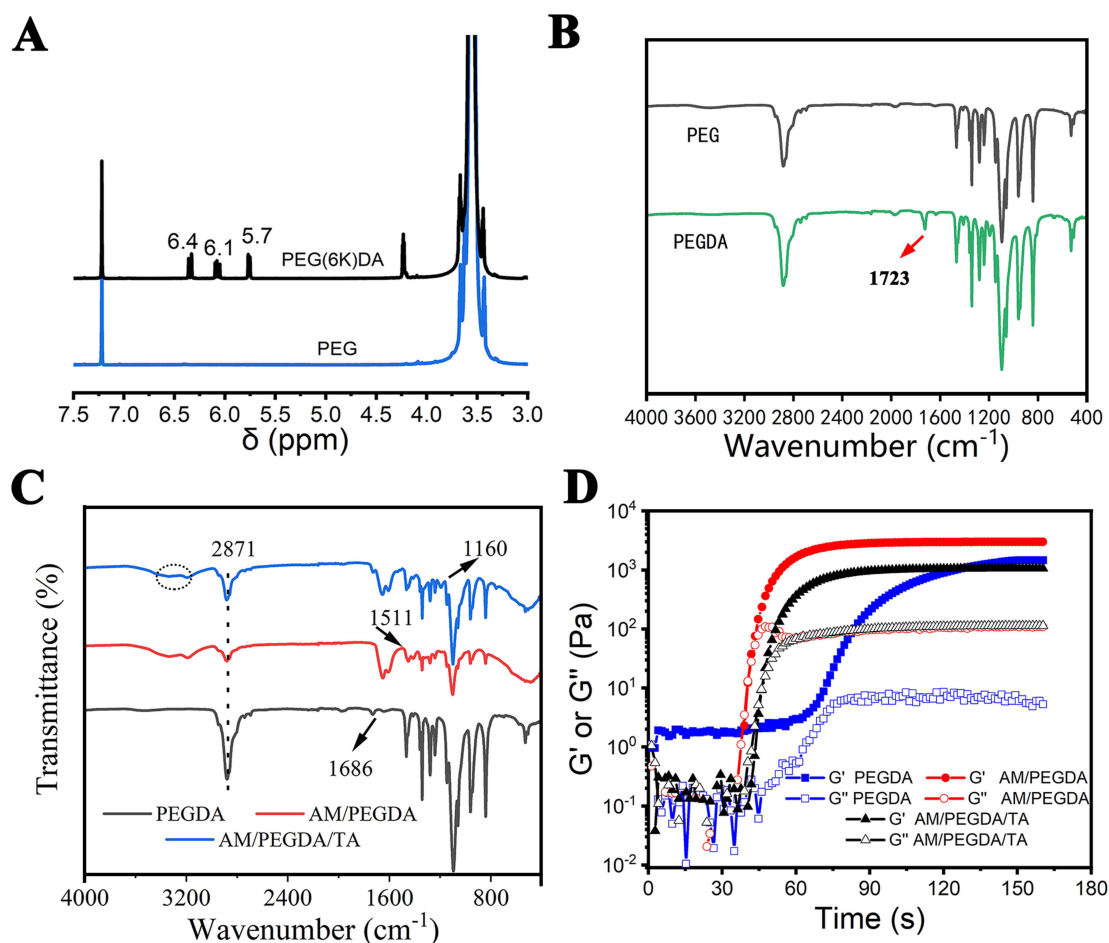

Figure 1 ^{1}H NMR spectrum (**A**) and FTIR spectrum (**B**) of PEG and PEGDA polymer. (**C**) FT-IR spectra of PEGDA monomer, AM/PEGDA/CS and AM/PEGDA/TA hydrogels. (**D**) Time sweeping tests under Blu-ray irradiance.

skeleton. Moreover, two new characteristic absorption peak signals are found at 1723 cm^{-1} and 1190 cm^{-1} from the PEGDA curve of FTIR spectrum (Figure 1B), which correspond to the C=O double bond and asymmetric C-O-C bond absorption peaks, respectively. These two vibration absorption peaks are the characteristic peaks generated after the PEG end groups are esterified by acyl chloride, which can further prove the success of the synthesis of PEGDA.

FTIR spectra (Figure 1C) were used to confirm the chemical structure of the composite hydrogels. The absence of the CH = CH$_2$ absorption peak at 1686 cm^{-1} in the curves of the AM/PEGDA and AM/PEGDA/TA hydrogels indicated that the reaction to cross-link the double bond had finished and that the covalent network had formed. The C-H stretching from PEG at 2882 cm^{-1}, which slightly changes to a lower wavenumber perhaps (around 2871 cm^{-1}) in AM/PEGDA/TA specimen due to the interaction between PEGDA and TA. While AM is definitely responsible for the peaks at 1404, 1453 and 1511 cm^{-1} corresponding to the amide I band,[36] and the broad peak at 3100–3400 cm^{-1} is attributable to the vibration of the phenolic hydroxyl group from TA or residual water molecules. A chemical reaction may be the cause of the acetal vibration peak at 1160 cm^{-1}. These modifications suggested that AM/PEGDA and TA interact intramolecularly during the complexation process.

Rheological measurements of the gelation process were carried out using time sweep. Different hydrogel systems' gelation processes were depicted in Figure 1D. The G' or G'' value showed the sol-gelation changeover point as it rapidly climbed from 0 to 150 s. The gelation time of PEGDA, AM/PEGDA, and AM/PEGDA/TA system was determined to be 74, 32, and 18s, respectively, and the corresponding equilibrium modulus was 2.1, 2.5, and 3.3 kPa. Due to the multiple crosslinking mechanism, the gelatin time of AM/PEGDA/TA hydrogel was quicker than that of the pure PEGDA sample and it had a greater equilibrium modulus (G_e').

Mechanical Performance of the Hydrogels

The AM/PEGDA/TA composite hydrogels showed higher mechanical strength and fatigue resistance compared to conventional hydrogels, which typically have lower compressive strengths and fatigue properties. Figure 2A and B depict typical compressive stress–strain curves and elastic modulus data for pure PEGDA, AM/PEGDA, and AM/PEGDA/TA hydrogels. The measurement findings showed that adding TA to the AM/PEGDA polymer network significantly boosted its mechanical strength, and that the superior mechanical performance was caused by the development of multiple-crosslinked structure, which led to an obvious increase in elastic modulus, augmenting from 16.2 kPa of AM/PEGDA to 31.4 kPa of AM/PEGDA/TA. Compared to the PEGDA (32 kPa) and AM/PEGDA (43 kPa) samples. The compressive strength of the AM/PEGDA/TA samples dramatically increased to 96 kPa.

It is clear from the tensile stress–strain curves in Figure 2C that the AM/PEGDA/TA hydrogels exhibit a substantial improvement in toughness. The representative AM/PEGDA/TA hydrogel could easily withstand much high deformation without any fracture, as evidenced by the tensile strengths of the AM/PEGDA and AM/PEGDA/TA hydrogels, which were increased over 3-fold over PEGDA hydrogel. Similar findings were made for the breaking strength hydrogel specimens (Figure 2D), which also confirmed the hydrogels' outstanding mechanical features (AM/PEGDA vs AM/PEGDA/TA). Correspondingly, the breaking strength of PEGDA, AM/PEGDA, and AM/PEGDA/TA hydrogel were 0.4 ± 0.1, 1.8 ± 0.7, or 2.6 ± 0.3 kPa, and their breaking strain was 77.8 ± 7.1, 331.2 ± 10.1, or 530.2 ± 12.7%, respectively.

SEM Observation and Adhesive of the Hydrogels

Scanning electron microscopy (SEM) was used to examine the microstructure of lyophilized hydrogels. Figure 3A and B show that the PEGDA hydrogels had loose pore structures with considerably larger pore sizes of around 267 ± 45 μm, while the AM/PEGDA/TA hydrogels had well-proportioned pore structures with the pore sizes of about 124 ± 19 μm. The porous structure network of connections helps cells transmit nutrients.[37] Due to the occurrence of several crosslinking mechanisms that result in better mechanical strength and a denser network structure, these results match the above mechanical attribute quite well.

Adhesive hydrogel dressings can prevent bacterial growth, reduce bodily fluid leakage, and lay the groundwork for hemostasis in addition to attaching and sealing to wounds.[38,39] Due to the presence of polyphenol groups, prior research has demonstrated that catechol-based hydrogels have a strong adhesive property to various surfaces. Based on a lap shear process, the final product exhibits good adhesive capacity to silicone rubber, plastic, stainless steel, porcine skin, and glass (Figure 3D). The AM/PEGDA/TA system has a greater ability to adhere to porcine skin than neat PEGDA and AM/
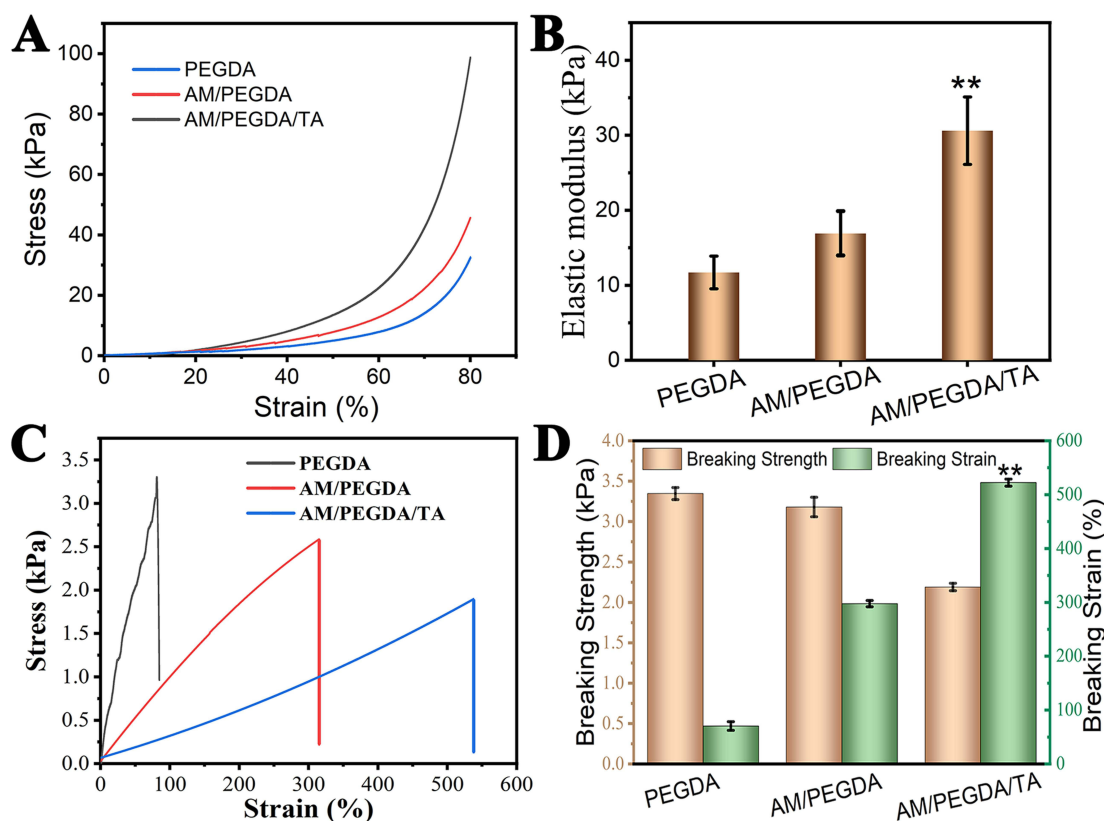
Figure 2 Mechanical properties of hydrogels. (**A**) Compression stress–strain curves of PEGDA, AM/PEGDA, and AM/PEGDA/TA scaffolds, and (**B**) their corresponding elastic modulus values. (**C**) Compression stress–strain curves of different hydrogels, and (**D**) their corresponding quantitative results of breaking strength and breaking strain. Statistical significance was analyzed by a one-way ANOVA. **$p < 0.01$.

PEGDA hydrogel (Figure 3C), and the adhesion strength of this system to tissues increases to 5.7 kPa, suggesting that the improvement in adhesion performance is primarily brought on by noncovalent or irreversible of covalent interactions of catechol-chemistry.[40]

Cytocompatibility Evaluation of Hydrogels in vitro

Potential cytotoxicity of the hydrogel dressings is another important consideration that influences their clinical applicability because they come into close touch with wound tissue.[41] As a result, the cytocompatibility assessments of HUVECs were carried out. The toxicity of the hydrogels was assessed using the live/dead staining technique and quantitative data from Image-J analysis, as shown in Figures 4A and B. Few dead cells were visible in the AM/PEGDA/TA groups, demonstrating the high biocompatibility of hydrogel system. As a result of the anti-cell adhesion for PEGDA polymer hydrogel, fewer cells show up in the PEGDA group than in the AM/PEGDA/TA group, whereas the number of cells increases noticeably with the addition of TA. Prior studies have shown that tough hydrogels are very resistant to cell attachment because they are often built on antifouling polymers like polyacrylamide and polyacrylates. Contrarily, we were able to change a tough hydrogel that was cell-repellent into a cell-adhesive hydrogel by adding TA to the hydrogel system. This represents a substantial advancement in the production of a tough hydrogel with good affinity to cells for real-world clinical applications.

Furthermore, cell morphology observations were carried out by using the staining assays to further investigate the biocompatibility of the manufactured scaffolds. After three days of growth, CLSM images revealed that the cells on the AM/PEGDA/TA hydrogels were easily distributed with extended filopodia, and they were joined by numerous HUVECs that adhered densely on the hydrogels to create a cell colony (Figure 4C). The PEGDA hydrogel without TA did not encourage cell attachment or spreading, as evidenced by the fact that cells on it scarcely spread and maintained
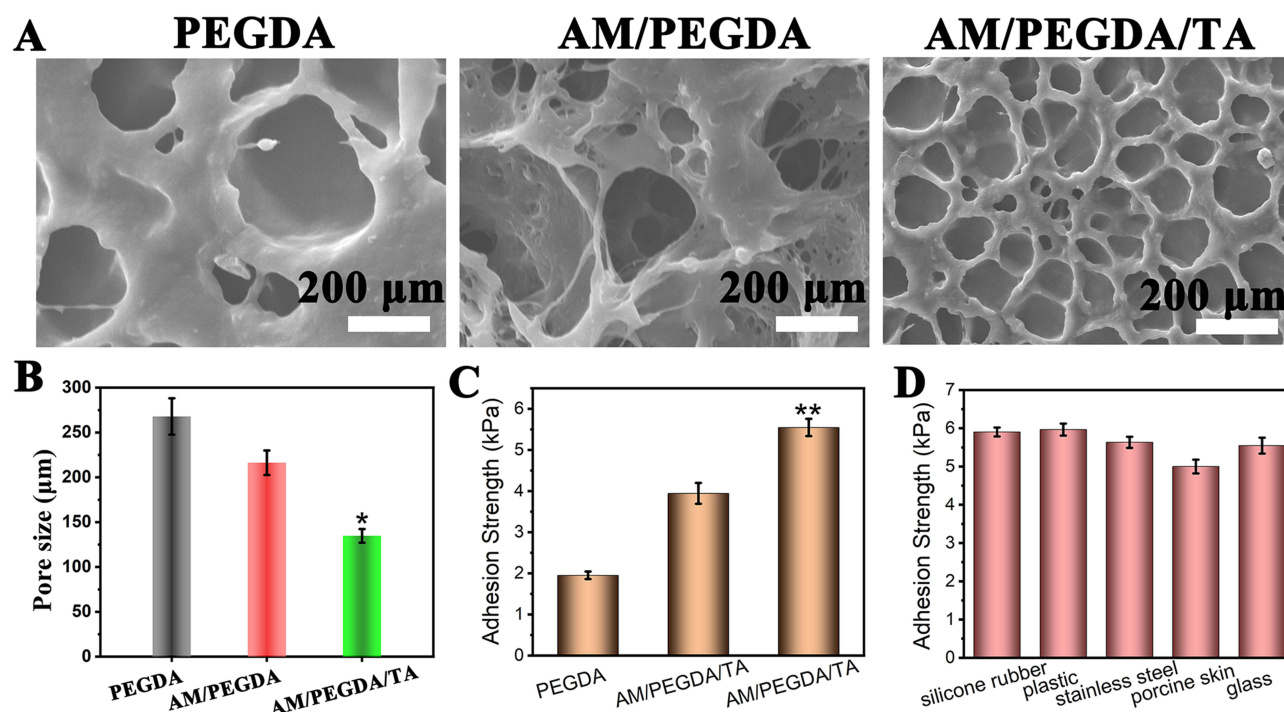
Figure 3 (**A**) SEM images of PEGDA, AM/PEGDA, and AM/PEGDA/TA hydrogel. (**B**) corresponding statistical pore size of different hydrogel samples. (**C**) Adhesion strength of PEGDA, AM/PEGDA, and AM/PEGDA/TA hydrogels adhered on porcine skin. (**D**) Adhesion strength of AM/PEGDA/TA scaffolds adhered on various substrates, including silicone rubber, plastic, stainless steel, porcine skin, and glass. Statistical significance was analyzed by a one-way ANOVA. $*p < 0.05$ and $**p < 0.01$.

a spherical shape during the whole culture period. In contrast to the PEGDA or AM/PEGDA hydrogels, more HUVECs were observed sticking to and spreading over the AM/PEGDA/TA hydrogel (Figure 4D), which may be explained by the interaction of the cells with the TA component. This was further confirmed using MTT, which highlighted the excellent cell viability of HUVECs cultivated on the hydrogel surface (Figure 4E). When compared to PEGDA and AM/PEGDA hydrogels throughout the culture period, the cell proliferation was increased for both AM/PEGDA and AM/PEGDA/TA hydrogels, which is attributed to the presence of TA and viscoelasticity of the composite hydrogel boosting cell adhesion and cell proliferation.[42]

Ability to Repair Full-Thickness Cutaneous Defect

The above results showed that the hydrogel had great potential to repair skin tissue due to its multifunctional properties. Then, a mouse full-thickness wound model was selected to assess the wound healing property of hydrogel in vivo. For comparison, PEGDA, AM/PEGDA, and AM/PEGDA/TA were dressed on the wound. Figure 5A shows representative images of the wound defects on the backs of mice in all three groups on days 0, 3, 7, and 10. It is obvious that the AM/PEGDA/TA hydrogel groups showed a faster wound contraction speed during the entire wound healing process. On the 3rd day, groups treated with AM/PEGDA, and AM/PEGDA/TA hydrogel showed wound area reduction to some extent, while the PEGDA group is still exhibited bigger wound area and the skin wound did not close at 7 days. After implantation of the scaffolds for 10 days, the wound areas treated with the AM/PEGDA/TA hydrogels were smaller than those by the PEGDA and AM/PEGDA groups. Meanwhile, the complete healing and coverage with the newly formed epidermis were observed for the wounds treated with the AM/PEGDA/TA sample at the end of treatment, showing a high wound closure effect. Figure 5B shows the comparison of the wound area analyzed with ImageJ software. It can be seen that the wounds in the neat PEGDA group healed very slowly, and 60% of the wound area still existed until the 10th day. The AM/PEGDA group had a moderate wound healing effect, while the AM/PEGDA/TA group possess obvious wound healing effect and its healing speed was comparable to that of the control group, and only 5% of the
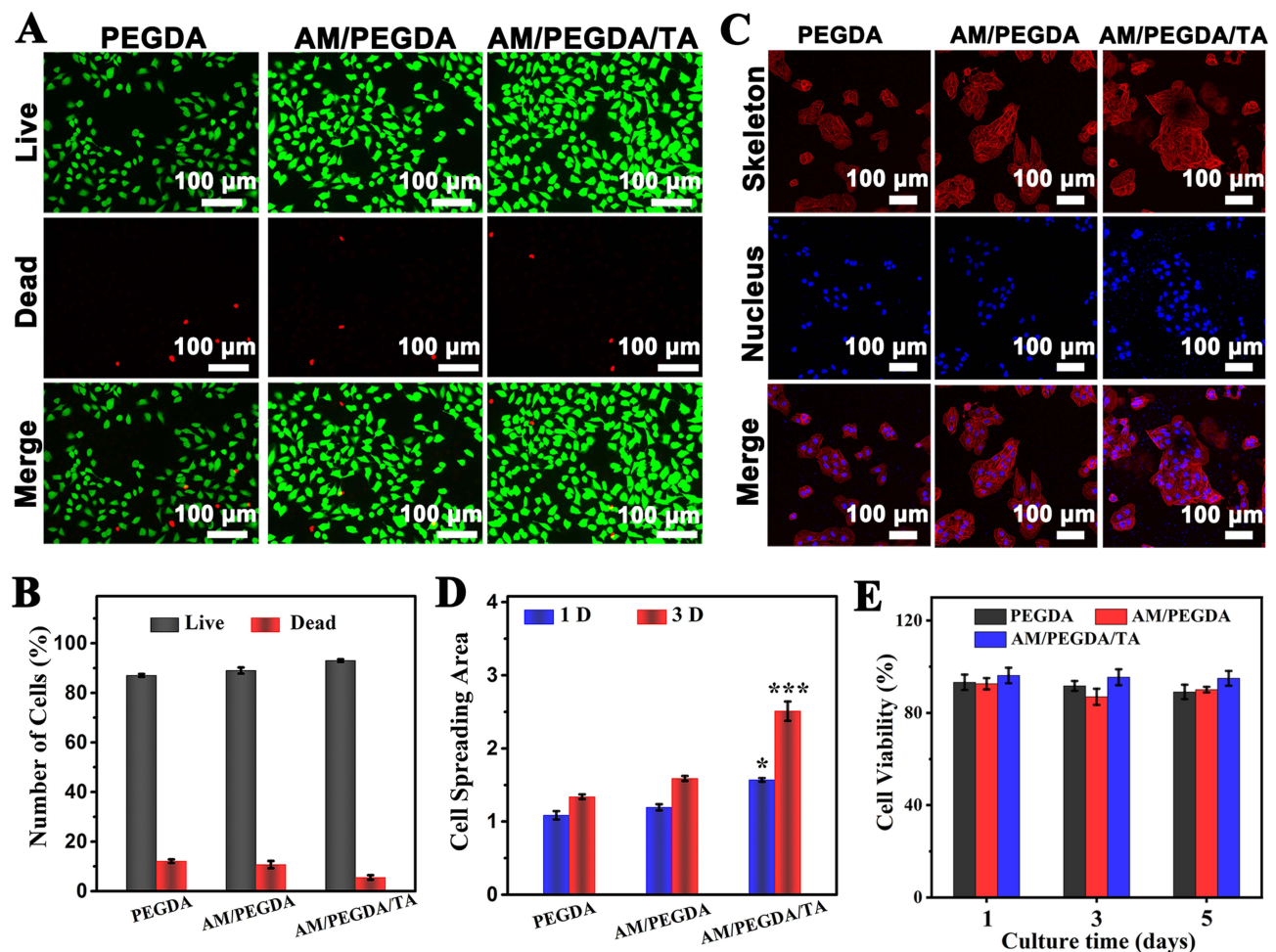
Figure 4 (**A**) Live/dead staining fluorescent images and (**B**) their quantitative analysis of live/dead cells of HUVECs after treatment with PEGDA, AM/PEGDA, and AM/PEGDA/TA hydrogels for 3 days. (**C**) CLSM images of stained HUVECs showing morphology cultivated on PEGDA, AM/PEGDA, and AM/PEGDA/TA scaffold and (**D**) their quantitative statistical spread area analysis on day 3. (**E**) Cell viability of HUVECs treated with various hydrogels by MTT assays. Statistical significance was analyzed by a one-way ANOVA. $*p < 0.05$, and $***p < 0.001$.

wound area remained on the 10th day. These results indicate that the introduction of TA can significantly promote wound repair.

To further explore the microscopic modifications of the wound healing process, the dermal tissues surrounding the original full-thickness wounds of the relevant groups on days 3 or 10 were taken and pathologically examined. According to the hematoxylin and eosin (H&E) staining photos (Figure 5C), the AM/PEGDA/TA hydrogel group had new epidermis (black arrow), and the dermis had been restored by a significant amount of connective tissue. Additionally, many fibroblasts (red dashed circle) were observed in AM/PEGDA/TA hydrogel group on 3rd day. The best skin healing result was particularly seen in the repaired tissue that had been subjected to AM/PEGDA/TA treatment for 10 days together with numerous blood vessels and newly generated hair follicles (red arrow). In contrast, the epithelial layer in the PEGDA and AM/PEGDA groups showed severe structural damage, and the AM/PEGDA group experienced partial epithelialization. After 10 days, the PEGDA groups showed significant inflammatory reaction and huge inflammatory cell infiltration (blue arrow), whereas the AM/PEGDA/TA hydrogel group showed numerous blood vessels and nearly complete skin tissue regeneration. Additionally, among these three groups, the dual-crosslinking hydrogel treated group displayed the thickest granulation tissue and increased hair follicle production (Figure 5D). These findings shown that the use of AM/PEGDA/TA hydrogel as a wound dressing can dramatically increase epidermal remodeling and facilitate wound healing.
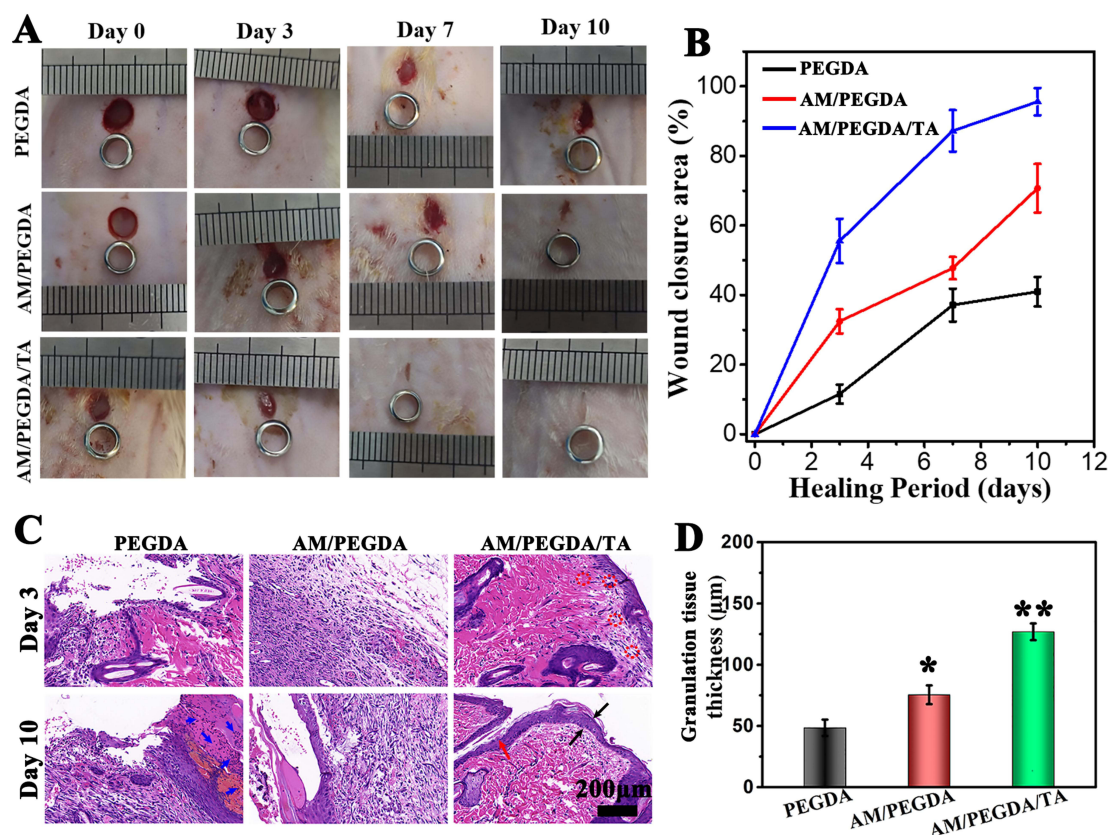
Figure 5 (**A**) Images of wound treated with PEGDA, AM/PEGDA and AM/PEGDA/TA formulations on days 0, 3, 7 and 10. (**B**) The corresponding healing rate of wound. (**C**) Representative images of H&E staining of wound tissues after treatment different dressings for days 3 and 10. Blue arrow represents inflammatory cell infiltration. Red dashed circle represents fibroblasts. Black arrow represents newly formed epidermis. Red arrow represents newly generated hair follicles. (**D**) Quantitative analysis of the granulation tissue thicknesses based on the Image J. Statistical significance was analyzed by a one-way ANOVA. *$p < 0.05$, **$p < 0.01$.

Anti-Inflammatory and Vascularization Efficacy of Hydrogels in vivo

Immunohistochemistry staining tests were conducted to learn more about the fundamental aspects of the healing process for wounds. Since one of the main factors impeding wound healing was an inflammatory response brought on by the wound infection, immunohistochemistry was used to assess the effectiveness of hydrogel dressings at preventing infections by measuring the expression of two common proinflammatory factors, IL-1β and IL-6. The PEGDA group had a significant amount of the two above-mentioned usual proinflammatory components. The AM/PEGDA/TA group displayed the lowest expression of proinflammatory markers (Figure 6), indicating that TA may aid in the healing of infected wounds. This is because TA also considerably increased the antibacterial, antioxidation, and adhesiveness of the composite hydrogel in a concentration-dependent manner, which were really helpful for hastening the healing process of wounds. As well as similar findings have been presented in previous studies.[39,43] Next, blood vessel density in vivo was measured using CD31 (a particular marker of vascular endothelium) staining assay. Due to the potential of the TA component to stimulate angiogenesis, only the AM/PEGDA/TA hydrogel treated group demonstrated enhanced neovascularization development. The AM/PEGDA/TA system, which had good anti-inflammatory performance, also helped create blood supply,[44] which greatly aided in the creation of neovascularization. Thus, the multiple-crosslinking hydrogel system created has a combined effect on controlling the inflammatory milieu and boosting angiogenesis, resulting in skin restoration.

Conclusion

In conclusion, we created a unique, remodeling, and biocompatible multifunctional wound and showed how it may be used to treat full-thickness skin wounds. The AM/PEGDA/TA hydrogel was created using a multiple-cross-linking
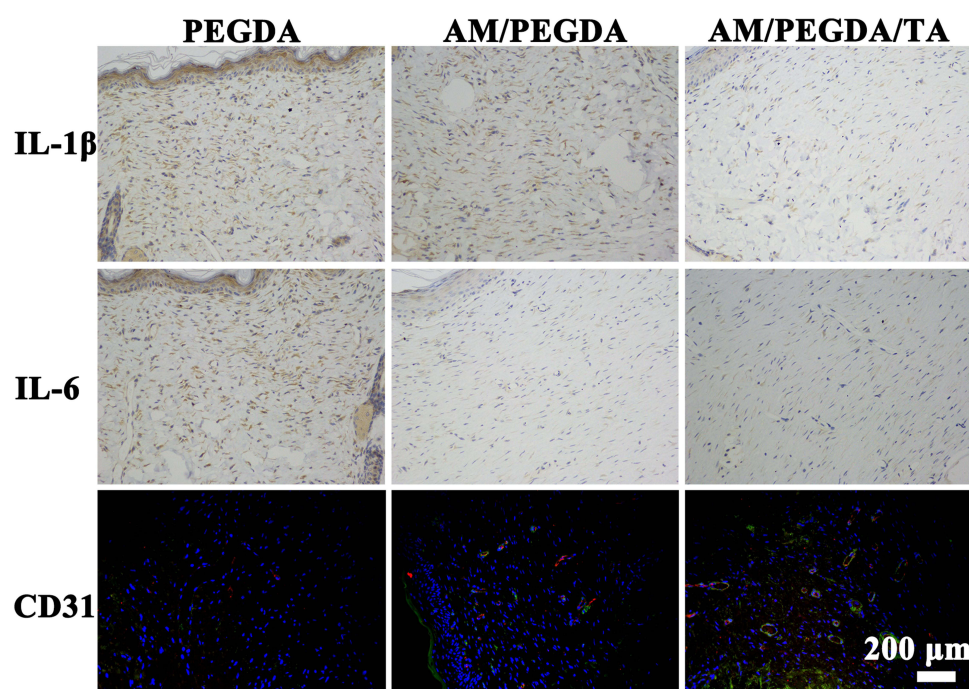
Figure 6 Immunohistochemical staining of pro-inflammatory factors IL-1β and IL-6 or double immunofluorescence staining of α-SMA (green) and CD31 (red) after different treatment for 10 days.

technique that involved double bond crosslinking, Schiff bases, and hydrogen bond interaction. This gave the hydrogel outstanding mechanical strength, strong tissue adhesion, and great biosafety. The resulting hydrogel dressings, when utilized as wound dressings, also had excellent shape adaptability, and because of their distinct gelling method, they can be flawlessly incorporated into the irregularly shaped wounds using an in situ forming approach. In a full-thickness wound model, the composite hydrogels significantly demonstrated excellent pro-reparative effects. The composite hydrogel enhanced collagen deposition, epithelium regeneration, vascularization, and down-regulated inflammatory level, which considerably accelerated the healing of skin wounds, according to the H&E, IL-1 or IL-6, and CD31 staining results. The composite hydrogel made it possible to integrate functions effectively, which made it the perfect choice for accelerating wound healing and identifying minute movements in the human body.

Acknowledgments

Disclosure

The authors declare no conflicts of interest in this work.

References

1. Huang L, Zhu Z, Wu D, et al. Antibacterial poly (ethylene glycol) diacrylate/chitosan hydrogels enhance mechanical adhesiveness and promote skin regeneration. *Carbohydr Polym*. 2019;225:115110. doi:10.1016/j.carbpol.2019.115110
2. Ahmadian Z, Correia A, Hasany M, et al. A Hydrogen-Bonded Extracellular Matrix-Mimicking Bactericidal Hydrogel with Radical Scavenging and Hemostatic Function for pH-Responsive Wound Healing Acceleration. *Adv Healthc Mater*. 2021;10(3):e2001122. doi:10.1002/adhm.202001122
3. Chen H, Cheng J, Cai X, et al. pH-Switchable Antimicrobial Supramolecular Hydrogels for Synergistically Eliminating Biofilm and Promoting Wound Healing. *ACS Appl Mater Interfaces*. 2022;14(16):18120–18132. doi:10.1021/acsami.2c00580
4. Cho JH, Lee JS, Shin J, et al. Ascidian-Inspired Fast-Forming Hydrogel System for Versatile Biomedical Applications: pyrogallol Chemistry for Dual Modes of Crosslinking Mechanism. *Adv Funct Mater*. 2017;28(6):1705244. doi:10.1002/adfm.201705244
5. Deng M, Zhang M, Huang R, et al. Diabetes immunity-modulated multifunctional hydrogel with cascade enzyme catalytic activity for bacterial wound treatment. *Biomaterials*. 2022;289:121790. doi:10.1016/j.biomaterials.2022.121790

6. Duan W, Liu X, Zhao J, Zheng Y, Wu J. Porous Silicon Carrier Endowed with Photothermal and Therapeutic Effects for Synergistic Wound Disinfection. *ACS Appl Mater Interfaces*. 2022;14(43):48368–48383. doi:10.1021/acsami.2c12012

7. Fu M, Zhao Y, Wang Y, et al. On-Demand Removable Self-Healing and pH-Responsive Europium-Releasing Adhesive Dressing Enables Inflammatory Microenvironment Modulation and Angiogenesis for Diabetic Wound Healing. *Small*. 2022:e2205489. doi:10.1002/smll.202205489

8. Haidari H, Bright R, Strudwick XL, et al. Multifunctional ultrasmall AgNP hydrogel accelerates healing of S. aureus infected wounds. *Acta Biomater*. 2021;128:420–434. doi:10.1016/j.actbio.2021.04.007

9. He J, Shi M, Liang Y, Guo B. Conductive adhesive self-healing nanocomposite hydrogel wound dressing for photothermal therapy of infected full-thickness skin wounds. *Chem Eng J*. 2020;394:124888. doi:10.1016/j.cej.2020.124888

10. Hu C, Long L, Cao J, Zhang S, Wang Y. Dual-crosslinked mussel-inspired smart hydrogels with enhanced antibacterial and angiogenic properties for chronic infected diabetic wound treatment via pH-responsive quick cargo release. *Chem Eng J*. 2021;411:128564. doi:10.1016/j.cej.2021.128564

11. Li C, Jiang T, Zhou C, et al. Injectable self-healing chitosan-based POSS-PEG hybrid hydrogel as wound dressing to promote diabetic wound healing. *Carbohydr Polym*. 2023;299:120198. doi:10.1016/j.carbpol.2022.120198

12. Li L, Cheng X, Huang Q, Cheng Y, Xiao J, Hu J. Sprayable Antibacterial Hydrogels by Simply Mixing of Aminoglycoside Antibiotics and Cellulose Nanocrystals for the Treatment of Infected Wounds. *Adv Healthc Mater*. 2022;11(20):e2201286. doi:10.1002/adhm.202201286

13. Li X, Luo S, Chen Y, et al. Facile One-Pot Synthesis of Meteor Hammer-like Au-MnOx Nanozymes with Spiky Surface for NIR-II Light-Enhanced Bacterial Elimination. *Chem Mater*. 2022;34(22):9876–9891. doi:10.1021/acs.chemmater.2c01775

14. Liang Y, Xu H, Li Z, Zhangji A, Guo B. Bioinspired Injectable Self-Healing Hydrogel Sealant with Fault-Tolerant and Repeated Thermo-Responsive Adhesion for Sutureless Post-Wound-Closure and Wound Healing. *Nanomicro Lett*. 2022;14(1):185. doi:10.1007/s40820-022-00928-z

15. Percival SL, Finnegan S, Donelli G, Vuotto C, Rimmer S, Lipsky BA. Antiseptics for treating infected wounds: efficacy on biofilms and effect of pH. *Crit Rev Microbiol*. 2016;42(2):293–309. doi:10.3109/1040841X.2014.940495

16. Wang Y, Zhou J, Yuan L, et al. Neighboring Carboxylic Acid Boosts Peroxidase-Like Property of Metal-Phenolic Nano-Networks in Eradicating Streptococcus mutans Biofilms. *Small*. 2022:e2206657. doi:10.1002/smll.202206657

17. Wu S, Yang Y, Wang S, et al. Dextran and peptide-based pH-sensitive hydrogel boosts healing process in multidrug-resistant bacteria-infected wounds. *Carbohydr Polym*. 2022;278:118994. doi:10.1016/j.carbpol.2021.118994

18. Huang L, Li W, Guo M, et al. Silver doped-silica nanoparticles reinforced poly (ethylene glycol) diacrylate/hyaluronic acid hydrogel dressings for synergistically accelerating bacterial-infected wound healing. *Carbohydr Polym*. 2023;304:120450. doi:10.1016/j.carbpol.2022.120450

19. Xuan Q, Jiang F, Dong H, et al. Bioinspired Intrinsic Versatile Hydrogel Fabricated by Amyloidal Toxin Simulant-Based Nanofibrous Assemblies for Accelerated Diabetic Wound Healing. *Adv Funct Mater*. 2021;31(49):2106705. doi:10.1002/adfm.202106705

20. Dong L, Zhang W, Ren M, et al. Moisture-Adaptive Contractile Biopolymer-Derived Fibers for Wound Healing Promotion. *Small*. 2023:2300589. doi:10.1002/smll.202300589

21. Wang A, Fan G, Qi H, et al. H_2O_2-activated in situ polymerization of aniline derivative in hydrogel for real-time monitoring and inhibition of wound bacterial infection. *Biomaterials*. 2022;289:121798. doi:10.1016/j.biomaterials.2022.121798

22. Suo H, Hussain M, Wang H, et al. Injectable and pH-Sensitive Hyaluronic Acid-Based Hydrogels with On-Demand Release of Antimicrobial Peptides for Infected Wound Healing. *Biomacromolecules*. 2021;22(7):3049–3059. doi:10.1021/acs.biomac.1c00502

23. Wang J, Chen XY, Zhao Y, et al. pH-Switchable Antimicrobial Nanofiber Networks of Hydrogel Eradicate Biofilm and Rescue Stalled Healing in Chronic Wounds. *ACS Nano*. 2019;13(10):11686–11697. doi:10.1021/acsnano.9b05608

24. Xian C, Zhang Z, You X, Fang Y, Wu J. Nanosized Fat Emulsion Injection Modulating Local Microenvironment Promotes Angiogenesis in Chronic Wound Healing. *Adv Funct Mater*. 2022;32(32):2202410. doi:10.1002/adfm.202202410

25. Zou CY, Lei XX, Hu JJ, et al. Multi-crosslinking hydrogels with robust bio-adhesion and pro-coagulant activity for first-aid hemostasis and infected wound healing. *Bio Mater*. 2022;16:388–402. doi:10.1016/j.bioactmat.2022.02.034

26. Zhao X, Liang Y, Huang Y, He J, Han Y, Guo B. Physical Double-Network Hydrogel Adhesives with Rapid Shape Adaptability, Fast Self-Healing, Antioxidant and NIR/pH Stimulus-Responsiveness for Multidrug-Resistant Bacterial Infection and Removable Wound Dressing. *Adv Funct Mater*. 2020;30(17):1910748. doi:10.1002/adfm.201910748

27. Zhao N, Yuan W. Functionally integrated bioglass microspheres-composited double-network hydrogel with good tissue adhesion and electrical conductivity for efficient wound treatment and health detection. *Composites, Part B*. 2022;242:110095. doi:10.1016/j.compositesb.2022.110095

28. Sahiner N, Sagbas S, Sahiner M, Silan C, Aktas N, Turk M. Biocompatible and biodegradable poly (Tannic Acid) hydrogel with antimicrobial and antioxidant properties. *Int J Biol Macromol*. 2016;82:150–159.

29. Chen F, Yu S, Liu B, et al. An injectable enzymatically crosslinked carboxymethylated pullulan/chondroitin sulfate hydrogel for cartilage tissue engineering. *Sci Rep*. 2016;6(1):1–12.

30. Jin R, Teixeira LSM, Dijkstra PJ, van Blitterswijk CA, Karperien M, Feijen J. Chondrogenesis in injectable enzymatically crosslinked heparin/dextran hydrogels. *J Controlled Release*. 2011;152(1):186–195.

31. Jin R, Hiemstra C, Zhong Z, Feijen J. Enzyme-mediated fast in situ formation of hydrogels from dextran–tyramine conjugates. *Biomaterials*. 2007;28(18):2791–2800.

32. O'Dwyer J, Murphy R, González-Vázquez A, et al. Translational Studies on the Potential of a VEGF Nanoparticle-Loaded Hyaluronic Acid Hydrogel. *Pharmaceutics*. 2021;13(6):779.

33. Huang J, Wu C, Yu X, Li H, Ding S, Zhang W. Biocompatible Autonomic Self-healing PVA-TA Hydrogel with High Mechanical Strength. *Macromol Chem Phys*. 2021;222(13):2100061.

34. Wu D, Yu Y, Tan J, et al. 3D bioprinting of gellan gum and poly (ethylene glycol) diacrylate based hydrogels to produce human-scale constructs with high-fidelity. *Mater Des*. 2018;160:486–495. doi:10.1016/j.matdes.2018.09.040

35. Hu D, Wu D, Huang L, et al. 3D bioprinting of cell-laden scaffolds for intervertebral disc regeneration. *Mater Lett*. 2018;223:219–222. doi:10.1016/j.matlet.2018.03.204

36. Huang L, Feng J, Zhu J, et al. A Strategy of Fenton Reaction Cycloacceleration for High-Performance Ferroptosis Therapy Initiated by Tumor Microenvironment Remodeling. *Adv Healthc Mater*. 2022:2203362. doi:10.1002/adhm.202203362

37. Jin Y, Koh RH, Kim SH, Kim KM, Park GK, Hwang NS. Injectable anti-inflammatory hyaluronic acid hydrogel for osteoarthritic cartilage repair. *Mater Sci & Eng C*. 2020;115:111096. doi:10.1016/j.msec.2020.111096

38. Zheng Z, Bian S, Li Z, et al. Catechol modified quaternized chitosan enhanced wet adhesive and antibacterial properties of injectable thermo-sensitive hydrogel for wound healing. *Carbohydr Polym*. 2020;249:116826. doi:10.1016/j.carbpol.2020.116826

39. He X, Liu X, Yang J, et al. Tannic acid-reinforced methacrylated chitosan/methacrylated silk fibroin hydrogels with multifunctionality for accelerating wound healing. *Carbohydr Polym*. 2020;247:116689. doi:10.1016/j.carbpol.2020.116689

40. Guo S, Ren Y, Chang R, et al. Injectable Self-Healing Adhesive Chitosan Hydrogel with Antioxidative, Antibacterial, and Hemostatic Activities for Rapid Hemostasis and Skin Wound Healing. *ACS Appl Mater Interfaces*. 2022;14(30):34455–34469. doi:10.1021/acsami.2c08870

41. Basha SI, Ghosh S, Vinothkumar K, et al. Fumaric acid incorporated Ag/agar-agar hybrid hydrogel: a multifunctional avenue to tackle wound healing. *Mater Sci & Eng C*. 2020;111:110743. doi:10.1016/j.msec.2020.110743

42. Zhang X, He Y, Huang P, et al. A novel mineralized high strength hydrogel for enhancing cell adhesion and promoting skull bone regeneration in situ. *Composites, Part B*. 2020;108183.

43. Guo S, Yao M, Zhang D, et al. One-Step Synthesis of Multifunctional Chitosan Hydrogel for Full-Thickness Wound Closure and Healing. *Adv Healthc Mater*. 2022;11(4):2101808. doi:10.1002/adhm.202101808

44. Eming SA, Brachvogel B, Odorisio T, Koch M. Regulation of angiogenesis: wound healing as a model. *Prog Histochem Cytochem*. 2007;42 (3):115–170. doi:10.1016/j.proghi.2007.06.001